

# 07. Filler-size-dependent dynamic mechanical properties of polyethylene glycol/zircon composites

*by Nur Aini Fauziah*

---

**Submission date:** 11-Feb-2022 10:23AM (UTC+0700)


**Submission ID:** 1759766551

**File name:** echanical\_properties\_of\_polyethylene\_glycolzircon\_composites.pdf (461.29K)

**Word count:** 7657

**Character count:** 37279

# Filler-size-dependent dynamic mechanical properties of polyethylene glycol/zircon composites

Nur Aini Fauziyah<sup>1,2</sup>  | Muthia Diah Nurmalarasi<sup>1</sup> | Allif Rosyidy Hilmi<sup>1</sup> |  
Triwikantoro Triwikantoro<sup>1</sup> | Malik Anjelh Baqiya<sup>1</sup> | Mochamad Zainuri<sup>1</sup> |  
Suminar Pratapa<sup>1</sup> 

<sup>1</sup>Department of Physics, Faculty of Sciences and Data Analytics, Institut Teknologi Sepuluh Nopember (ITS), Surabaya, Indonesia

<sup>2</sup>Department of Chemical Engineering, Faculty of Engineering, Universitas Pembangunan Nasional "Veteran" Jawa Timur (UPN), Surabaya, Indonesia

## Correspondence

Suminar Pratapa, Department of Physics, Faculty of Sciences and Data Analytics, Institut Teknologi Sepuluh Nopember (ITS), Sukolilo, Surabaya 60111, Indonesia.  
Email: suminar\_pratapa@physics.its.ac.id

## Funding information

Ministry of Research and Technology/BRIN of the Republic of Indonesia, Grant/Award Number: 1055/PKS/ITS/2021

## Abstract

The thermomechanical properties of polyethylene glycol (PEG) composites filled with various zircon sizes were studied. The zircon powders were derived from natural (well-known as puya) sand collected from Kereng Pangi, Central Kalimantan, Indonesia. The effects of the zircon size and content were examined to understand the thermomechanical properties of the composites using dynamic mechanical analysis in shear mode. Pure zircon powders with micron to nanometer sizes were prepared. The microzircon powders were prepared by heating zircon at 500, 1000, and 1200°C. Moreover, the nanozircon powders were prepared by a wet milling method with milling times of 5, 10, and 15 hours. Furthermore, the composites were prepared by a wet mixing method. According to elemental analysis of scanning electron microscopy/energy dispersive X-Ray spectroscopy (SEM/EDX) data, it was found that the various zircon sizes caused different distribution effects, that is, in general, the smaller the size was, the better the distribution. Filler size variation also affected the thermomechanical properties of the composites. The addition of microzircon heated at 1200°C had the lowest storage moduli ( $G'$ ), that is, 154.90 MPa and 155.55 MPa for 5 wt.% and 10 wt.%, respectively. Moreover, the maximum value of  $G'$  was obtained for the composite with the addition of nanozircon milled for 10 h (Z10h), that is, 679.27 MPa and 706.37 MPa for 5 and 10 wt.%, respectively. The addition of nanozircon slightly reduced room-temperature  $G'$ , presumably due to the agglomerated filler, as confirmed by the SEM/EDX data. Moreover, a decrease in zircon size caused an increase in the melting temperature ( $T_m$ ) of the matrix. In contrast, 15 h of milling had a minor effect on  $T_m$  and  $G'$ , whereas the loss modulus ( $G''$ ) decreased with the addition of nanozircon. The effects of filler size on the thermomechanical properties of PEG/zircon composites are discussed in detail.

## KEYWORDS

nano- and micron-sized filler, PEG, thermomechanical properties, zircon

## 1 | INTRODUCTION

In recent years, the use of ceramic powders to enhance the strength of polymers has been of concern to many researchers because the results are composites with outstanding properties. There are many factors influencing the improvement, including the concentration of filler, filler size,<sup>1–4</sup> dispersion of filler in the matrix,<sup>5,6</sup> and interfacial interaction between the filler and matrix.<sup>7,8</sup> These effects are important for a wide range of scientific and industrial processes.

One abundantly available and easy-to-process ceramic powder is zircon (ZrSiO<sub>4</sub>). A pure zircon powder can be obtained by a facile route from zircon sand.<sup>9</sup> Its high hardness (7.5 Mohs  $\approx$  13.475 GPa<sup>10</sup>), low thermal expansion ( $4.1 \times 10^{-6}/^{\circ}\text{C}$ ) between 20°C and 1000°C,<sup>10</sup> and high dissociation temperature (1675°C)<sup>11</sup> make it suitable as a filler of polymer matrix composites where thermal and mechanical loading is applied. Previously, we reported the synthesis of pure zircon powders<sup>9,12</sup> with an as-product crystallite size of approximately 170 nm.

There are approaches to obtain ceramic powders with different sizes. In general, heating will result in a larger crystallite size owing to crystal growth. Size reduction, however, is more complicated. Researchers have introduced milling as a simple one. For example, Chauruka et al.<sup>13</sup> examined the effectiveness of particle size reduction by air jet milling in reducing the particle size of  $\gamma$ -alumina from 37  $\mu\text{m}$  to 2.9  $\mu\text{m}$ . Moreover, Dawei et al.<sup>14</sup> prepared nanozircon by a microwave-hydrothermal method at 160–200°C for 30 min, in which a mineralizer was needed to promote crystallite growth. Furthermore, Musyarofah<sup>9</sup> succeeded in obtaining zircon sizes up to  $\sim$ 40 nm by wet milling for 10 h. Therefore, 170 nm zircon powder<sup>9</sup> can potentially be formed into nanozircon powders by milling and submicrozircon powders by heating. In our previous study,<sup>15</sup> we reported the PEG/(5 wt.%) microzircon and found that the highest storage modulus was achieved by composites with a microzircon heated at 500°C. However, the effect of zircon size (from micro to nanozircon) on the thermomechanical properties of polymer matrix composites, where polyethylene glycol is used as the matrix, has not been thoroughly investigated.

In this study, the effect of zircon filler size on the thermodynamic properties of PEG/zircon composites will be determined by dynamic mechanical analysis (DMA) in shear mode. The zircon size is varied using milling and heating. The effect of milling on the microstructure of the powder is considered. The distribution of fillers in the PEG matrix will also be investigated from Scanning Electron Microscopy/Energy Dispersive X-Ray (SEM/EDX) characterization. The zircon powder was extracted from zircon sand from Kereng Pangi, Central Kalimantan, Indonesia.

## 2 | EXPERIMENTAL

### 2.1 | Materials

The matrix used was polyethylene glycol (PEG4000) purchased from Merck (Hohenbrunn, Germany). The filler used was natural zircon sand (well-known as puya sand) from Kereng Pangi, Central Kalimantan, Indonesia, locally purified in our laboratory. We also added a dispersion agent, sodium dodecyl sulfate salt (SDS), provided by MerckKGaA, Germany.

Zircon purification was carried out in three main processes, that is, magnetic separation, immersion in HCl, and reaction with NaOH. The purification processes are reported in detail in the reference.<sup>9</sup> The resulting pure zircon (170 nm in size) was then transformed to nanometer size using a top-down method via wet ball milling by varying the milling time for 5, 10, and 15 h, followed by drying and annealing at 200°C for 1 h to reduce or eliminate the nonuniform residual strain of the milled powders. Moreover, submicrozircon was prepared by heating pure zircon powder at 500°C, 1000°C, and 1200°C to allow zircon crystallite growth. Table 1 presents the nomenclature of the zircon samples.

### 2.2 | Preparation of the composites

The composites were prepared first by melting PEG at 60°C. As much as 0.2 wt.% SDS was then added to the melted PEG

TABLE 1 Summary of sample nomenclature and descriptions

Sample symbol	Description
Z1200	pure zircon powder heated at 1200°C
Z1000	pure zircon powder heated at 1000°C
Z500	pure zircon powder heated at 500°C
Z0	original pure zircon powder (crystallite size of 185 nm)
Z5h	pure zircon powder milled for 5 h
Z10h	pure zircon powder milled for 10 h
Z15h	pure zircon powder milled for 15 h
P/Z1200	PEG-based composite filled with Z1200
P/Z1000	PEG-based composite filled with Z1000
P/Z500	PEG-based composite filled with Z500
P/Z0	PEG-based composite filled with Z0
P/Z5h	PEG-based composite filled with Z5h
P/Z10h	PEG-based composite filled with Z10h
P/Z15h	PEG-based composite filled with Z15h

prior to dispersion of the designated zircon powder in the PEG matrix. Under liquid conditions, as much as 5 and 10 wt.% zircon powder (with a certain crystallite size) was added to form a PEG/zircon composite. Finally, the composites were cast in the geometry for shear mode measurements: 1 mm thickness and 5 mm × 5 mm squares. The detailed sample preparation has also been described before.<sup>12</sup> Table 1 presents the nomenclature of the composite samples.

The cast samples were subjected to DMA measurement to examine their thermomechanical properties with a temperature range of 30–80°C and a heating rate of 5°C min<sup>-1</sup>.

## 2.3 | Characterizations

### 2.3.1 | X-ray diffraction (XRD)

The phase analysis was carried out by XRD data (Philips X'Pert MPD diffractometer over the 2θ range of 15–65°; Cu-Kα radiation: λ = 0.154056 nm at 40 kV and 30 mA). The quantitative analysis of XRD data was performed using *Rietica* dan *MAUD* programs, which apply the XRD whole-pattern Rietveld method.

### 2.3.2 | Scanning and transmission electron microscopy (SEM/TEM)

An SEM (Carl Zeiss) instrument with EDX was used to observe the morphology and zircon distribution in the PEG matrix by revealing the map of each element. These measurements were observed at 20 kV in secondary electron imaging mode. The zircon powders were observed using TEM (FEI Tecnai-T20) with 680 mm camera length and bright field image mode at 200 kV tension.

### 2.3.3 | Fourier transform infrared (FTIR) spectroscopy

FTIR was used to characterize the intermolecular bonding in the zircon, PEG, and composite samples at wavenumbers from 4000 to 400 cm<sup>-1</sup>. Here, we used a Bruker Vertex7.0v FTIR spectrometer.

### 2.3.4 | Dynamic mechanical analyzer (DMA)

The thermomechanical behavior of the pure PEG and the composites were characterized using a DMA/SDTA861e Mettler Toledo instrument in shear mode (approximately 25°C [room temperature] to 80°C with oscillation response at 1 Hz). Here, the DMA observation

followed ASTM D4065 for the shear mode. We were concerned with the shear  $G'$  storage moduli,  $\tan \delta$  (damping factor), and loss moduli ( $G''$ ). Moreover, we determined the melting temperature ( $T_m$ ) of the composites from the  $\tan \delta$  peak. For PEG-based composites, it has been confirmed that the results were equal to DSC measurements.<sup>16,17</sup>

## 3 | RESULTS AND DISCUSSION

### 3.1 | Synthesis of zircon powder with various sizes

Figure 1 shows the XRD patterns of zircon powders after heating and milling. All samples show a pure zircon phase with different peak broadening characteristics. Furthermore, the XRD data were subjected to Rietveld-based analyses to reveal the crystallite size and non-uniform strain of the present phase. This microstructural information can be related to XRD peak broadening, as also reported in a previous study.<sup>18</sup> A peak broadening indicates a smaller crystal size but could be due to its combination of a larger residual nonuniform strain. As seen in Table 2, heating produces a larger zircon crystallite size but relatively the same strains. This result confirms that tailoring the crystallite size can be done by applying heating, particularly by making use of the “grain growth” approach for ceramics. The broad use of the term crystallite size is usually equated with a domain

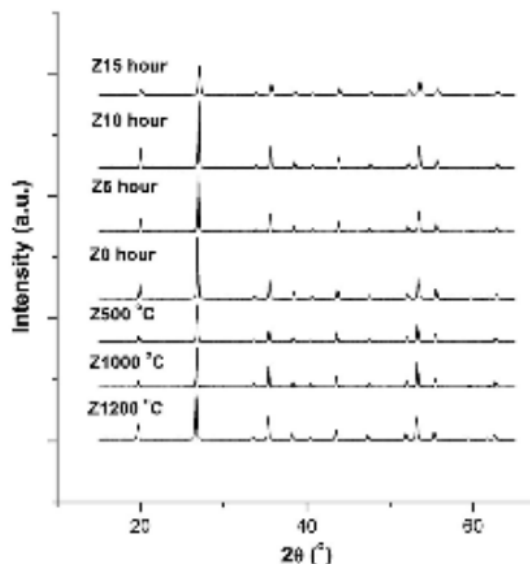


FIGURE 1 XRD patterns (Cu-Kα radiation) of zircon powders with varied zircon sizes

containing single crystals in powder form, while grains are the same but in bulk form. The former is usually estimated using Scherrer's equation<sup>19</sup> from diffraction data, while the latter is observed using electron microscopy. Moreover, particle size refers to agglomerated powders. The table also shows that milling reduces zircon crystallite size but at the same time increases its residual nonuniform strain. During milling, zircon powder was subjected to severe friction and impact with milling balls and the wall of the milling jar. Long or rapid milling provides a great amount of friction and impact energy, which eases hard powders to deform and then break up. Deformation causes residual strains and the powder breaks up, resulting in a smaller powder size. As seen from Table 2, the zircon crystallite size decreases to

TABLE 2 Output of quantitative analysis of the XRD data of zircon powders (referred to Figure 1) using the Rietveld-based MAUD program to extract microstructural data

Samples	Crystallite size (nm)	Nonuniform residual strain ( $10^{-4}$ )
Z1200	391	2.4
Z1000	321	2.7
Z500	226	2.9
Z0h	185	3.2
Z5h	174	3.9
Z10h	50	8.5
Z15h	33	9.3

Note: All samples exhibit single-phase crystallites, that is, zircon.

approximately one-third of its original size, ca. 33 nm after 15 h of milling, but its residual strain is contrariwise tripled. These results are similar to previous research.<sup>9</sup> We notice that further milling does not effectively reduce zircon size, and therefore, 15 h is used as the maximum milling time. To confirm the size variation of zircon, we collected TEM images of the powders (Figure 2) and found almost similar results for zircon sizes. We conclude that zircon powders, as a candidate of PEG filler, with varying sizes from 33 to 391 nm have been successfully prepared using milling or heating techniques.

The microstructure of zircon powder was further examined by SEM images (Figure 3) to reveal the morphology of its grains. There was a clear decrease in grain size from the Z1200 to Z15h samples. Zircon powders have an irregular platelet morphology after milling. A longer milling time causes flattening of the zircon powder, indicating the presence of severe residual strains. Moreover, heating does not affect the morphology of the powder compared to the untreated powder (sample Z0), except for the increased size. This microstructural observation is in accordance with the previous discussion on XRD data.

### 3.2 | Synthesis of PEG/zircon with various zircon sizes

The successful preparation of zircon powders of various sizes was followed by the synthesis of PEG/zircon composites. We used XRD and FTIR methods to investigate

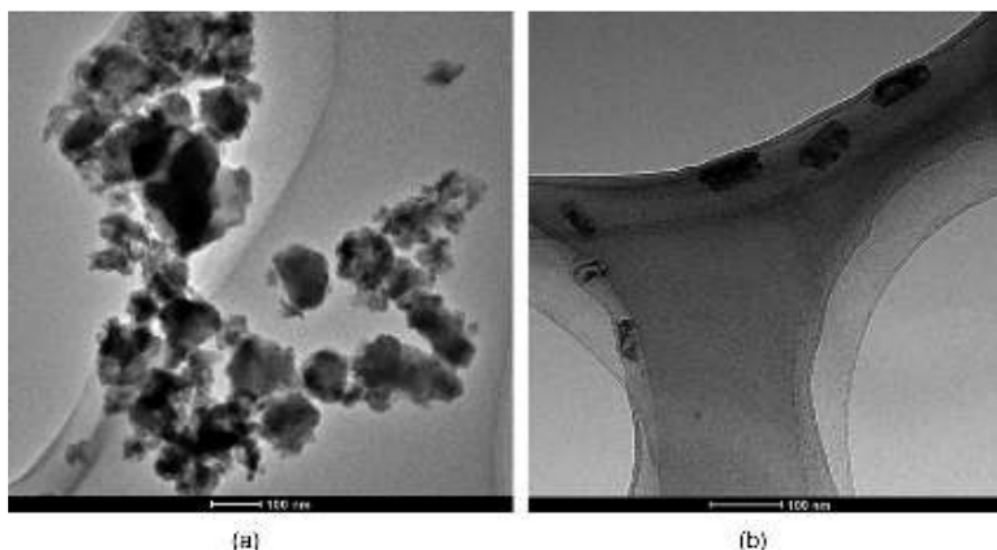
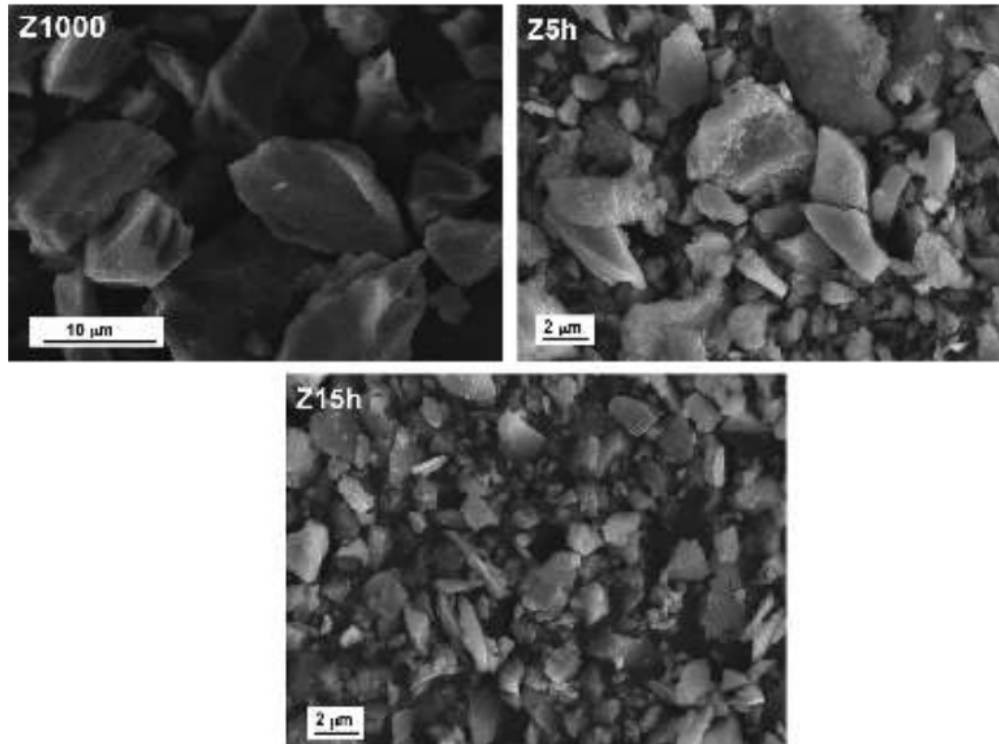
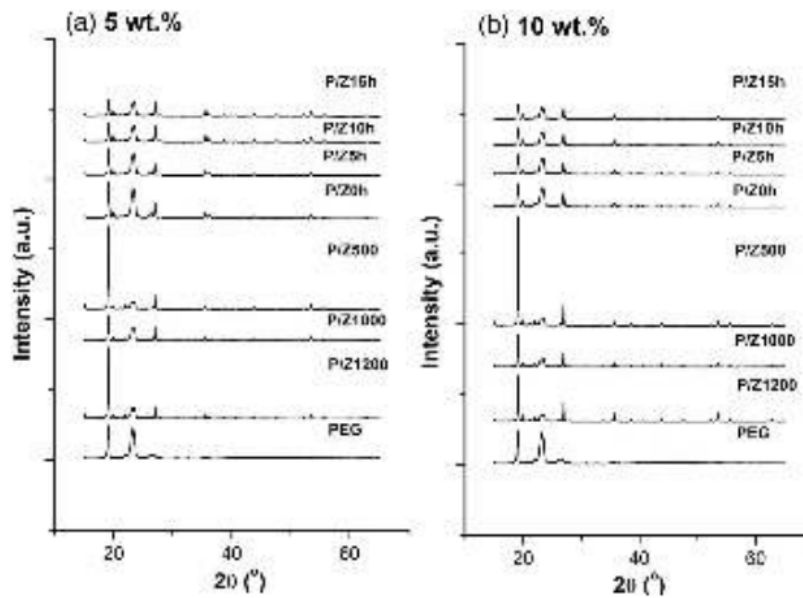


FIGURE 2 TEM images of zircon powders (a) Z0h and (b) Z15h



**3** FIGURE 3 SEM images of zircon powders (a) Z1000, (b) Z5h, and (c) Z15H

FIGURE 4 XRD patterns (Cu K $\alpha$  radiation) of PEG/zircon composites with varied zircon size and content of (a) 5 wt.% and (b) 10 wt.%



the attainment of the composites. We find no new peaks due to the formation of zircon-PEG composites. All peaks from XRD (Figure 4) and FTIR (Figure 5) independently

belong to PEG and zircon phases. For example, the XRD main peaks of PEG are found at  $2\theta \approx 19.10^\circ$  and  $23.23^\circ$ , and those of zircon are found at  $2\theta \approx 19.72^\circ$ ,  $26.69^\circ$ , and

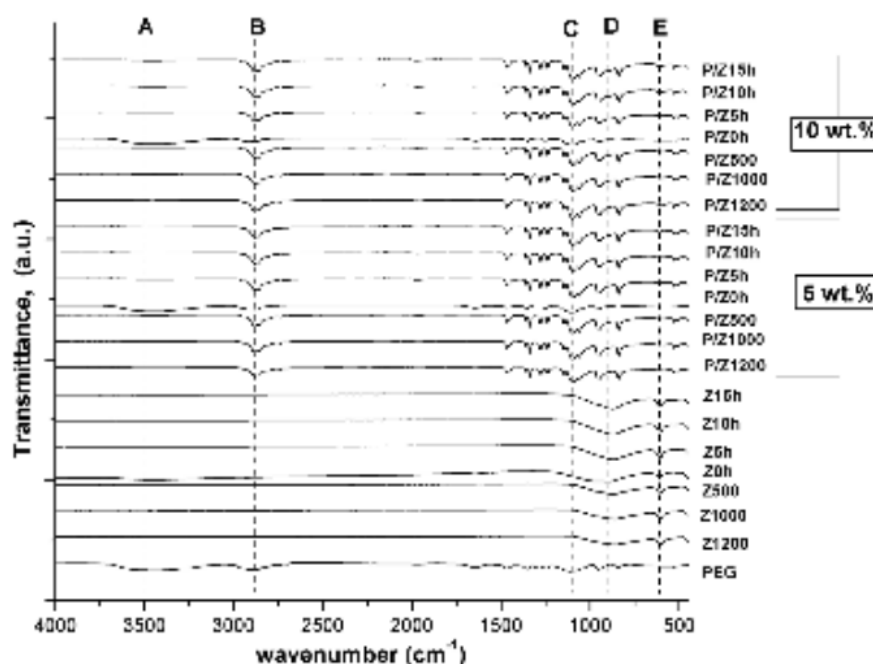


FIGURE 5 FTIR spectra of PEG/zircon composites with varied zircon size and content

35.36°. The XRD peaks exhibit no significant  $2\theta$  shift after the synthesis of the composites, but the intensity of zircon peaks decreases with the addition of nanozircon. This result was in line with the XRD pattern of zircon powder (Figure 1). Moreover, the more filler composition added, the higher the intensity of zircon. This indicates that there is no reaction between PEG and zircon. Moreover, the FTIR spectra of the samples (Figure 5) consisted of peaks from PEG (denoted as A, B, and C) and zircon (D and E). Further analysis is carried out by comparing the infrared wavenumber data of all PEG/zircon composites, which are shown in Figure 5. All composites (with compositions of 5 wt.% and 10 wt.% zircon) show a broad absorption peak at  $612\text{ cm}^{-1}$  due to Zr–O bending (assigned as E), and the peak at  $840\text{ cm}^{-1}$  (assigned as D) corresponds to the presence of Si–O–Si stretching. Moreover, the main peaks of PEG at  $2882\text{ cm}^{-1}$  and  $3500\text{ cm}^{-1}$  (assigned as B and A, respectively) are formed by O–H stretching of hydroxyl groups on the surface of PEG.<sup>20</sup> The other absorption band at  $1097\text{ cm}^{-1}$  is attributed to C–O–C symmetric stretching from the PEG matrix (assigned as C). Interestingly, milling and heating treatments do not significantly shift the wavenumber of the zircon spectra, which is in line with earlier findings.<sup>21</sup> Moreover, the peak intensity of nanozircon-filled PEG composites is slightly higher than that of microzircon composites. It appears that nanozircon powder fills the free volume of PEG more effectively than microzircon powder. The

more nanozircon particles incorporated in PEG, the higher the vibrational absorption of the infrared spectra. Overall, these results confirm the formation of PEG/zircon composites with different zircon sizes. This finding also completes our previous work.<sup>12</sup>

### 3.3 | Morphology and distribution of zircon in the PEG matrix

Figure 6 presents SEM images of the surface of three representative composites without zircon filler and with micro and nanozircon fillers. The influence of zircon size on the matrix is clear. In Figure 6(a), composite P/Z500 with microzircon filler has a wrinkle and loose surface. The composite surface is more compact when filled with a nanosized filler, as shown in Figure 6(c), although it tends to agglomerate. Further studies were carried out using SEM/EDX to determine the distribution of zircon in PEG (Figure 7). The distribution is crucial since it is an important factor that may affect the thermomechanical properties of the composites.<sup>16</sup> In Figure 7, red, green, blue, and yellow dots represent silicon, oxygen, carbon, and zirconium elements. Elemental distribution observations can be qualitatively confirmed using a graph of the pixel values according to a linear distance. The intensity of a pixel represents the amount of an element in the pixel. Figure 7(d) and (e) show the graph for Zr. Well-dispersed Zr is represented by regular

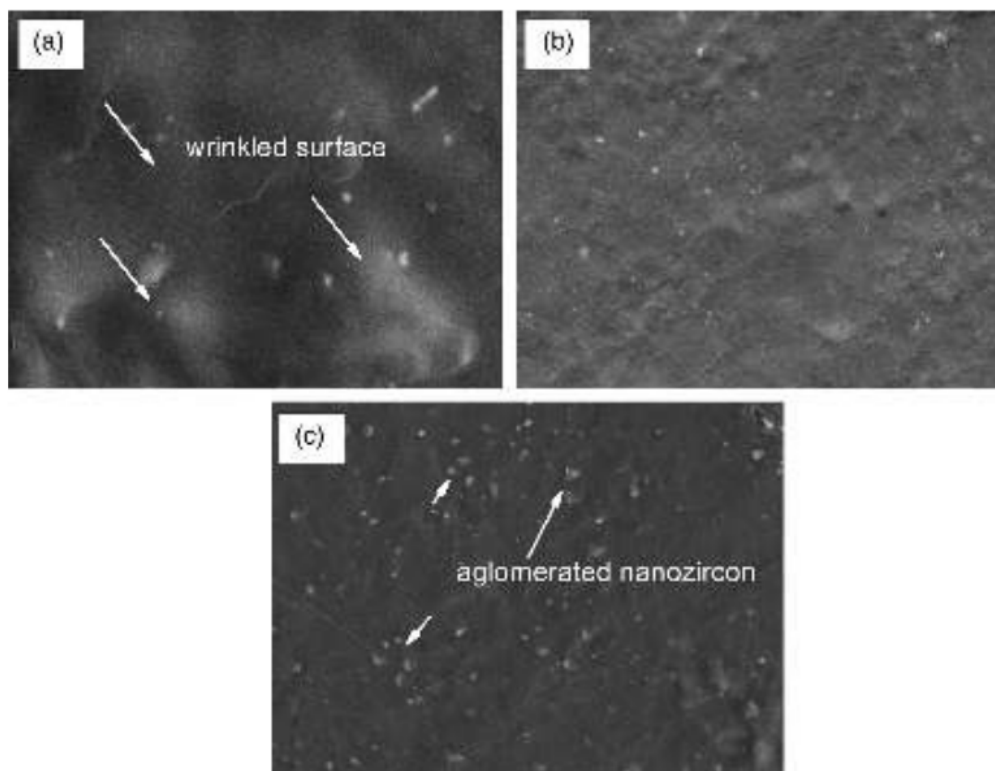


FIGURE 6 SEM surface morphology of PEG/zircon (a) P/Z500, (b) P/Z0, and (c) P/Z15h composites

peaks across the spatial distance. According to this qualitative approach for Figure 7, P/Z15h would have the best zircon distribution. To provide a complete explanation of the distribution of zircon fillers in all composites, a quantitative approach is used. Since we are concerned with the zircon distribution, we can spot the line distribution of Zr using *PixelProfile* software in the PEG matrix and analyze the dispersibility index ( $I_{dispersibility}$ ) using equations in previous studies.<sup>5,16</sup> A lower  $I_{dispersibility}$  index in this case means a well-distributed zircon.

The complete zircon distribution analysis results are shown in Table 3. The lowest  $I_{dispersibility}$  value is shown by the sample with the Z10h filler, that is, with a zircon size of 50 nm. At first glance, a large microzircon will be a barrier to the movement of the others during mixing, which results in a low zircon distribution in the PEG matrix. In contrast, as demonstrated by the nanozircon filler composites, the smaller the zircon size is, the more homogeneous the zircon distribution is. However, zircon sizes lower than 50 nm would result in agglomeration, as indicated by the increase in the  $I_{dispersibility}$  value for sample Z15h. This result is consistent with the SEM observation for the nanozircon powders (Figure 6(c)). Figure 8 represents the mechanism of the reinforcement from

micro and nanozircon filler in PEG. In our experiment, SDS was used as the dispersant agent. It was expected to initiate better adsorption of sulfate polar groups on the zircon surface by electrostatic interactions and improved zircon distribution as previously observed in PEG/silica composites.<sup>16,22</sup> Since the  $I_{dispersibility}$  values of the nanozircon is smaller than that of the microzircon, we argue that the effect of SDS in dispersing zircon as filler is more pronounced for the former than the latter.

### 3.4 | Storage modulus

Figure 9 shows the effects of zircon size on the temperature-dependent shear storage moduli ( $G'$ ) of the PEG/zircon composites for two different zircon compositions, that is, 5 and 10 wt.%. The effect of the filler size has an important role in the thermomechanical properties of a composite. To clarify this effect, the figures are presented in two parts, that is, the original and heated fillers (Figure 9(a) and (b)) and the original and milled-annealed fillers (Figure 9(b) and (d)). The effect is first considered from the fact that the shear moduli of the composites gradually decline with temperature. This



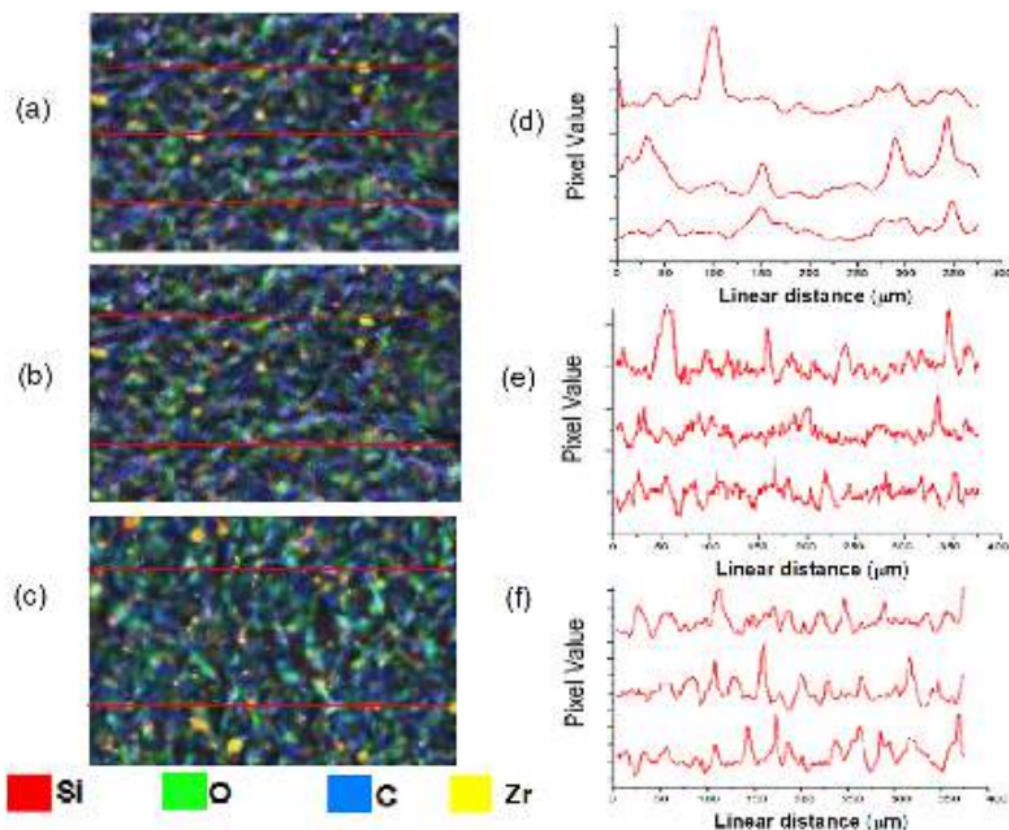


FIGURE 7 SEM-EDX micrographs and elemental maps for some representative samples of PEG/zircon composites (in various size) (a) P/Z500, (b) P/Z0, and (c) P/Z15h. The horizontal lines are presented to show Zr distribution by PixelProfile analysis, and line profile values show on (d) P/Z500, (e) P/Z0, and (f) P/Z15h [Color figure can be viewed at wileyonlinelibrary.com]

TABLE 3 Average dispersibility index values ( $I_{dispersibility}$ ) of PEG/zircon composites with varied zircon size and content

Samples	$I_{dispersibility}$	
	5 wt. %	10 wt. %
P/Z1200	0.397	0.390
P/Z1000	0.393	0.386
P/Z500	0.384	0.371
P/Z0h	0.343	0.340
P/Z5h	0.253	0.251
P/Z10h	0.237	0.235
P/Z15h	0.249	0.247

reduction is divided into three areas that are common in PEG-based composites,<sup>16</sup> that is, rubbery state (around the ambient temperature to 40°C) with a slight decrease, melting area (starting from 40°C up to 60°C) with a sharp decline, and liquid area (more than 60°C). First, at ambient temperature, the  $G'$  values of the composites are

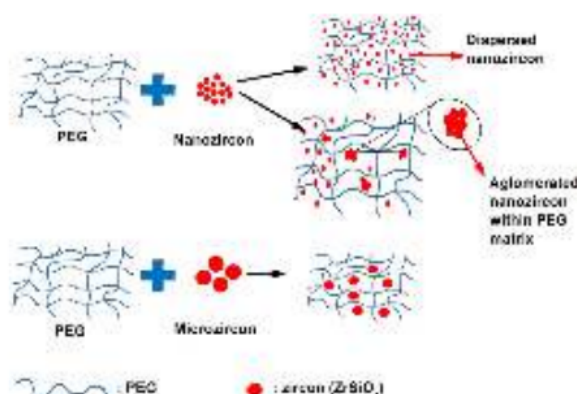


FIGURE 8 Reinforcement mechanism on the PEG/zircon composites with micro or nanozircon fillers [Color figure can be viewed at wileyonlinelibrary.com]

higher than that of pure PEG. Furthermore, they differ in terms of zircon (a) size, (b) dispersibility, and (c) composition. At this temperature, there is a clear

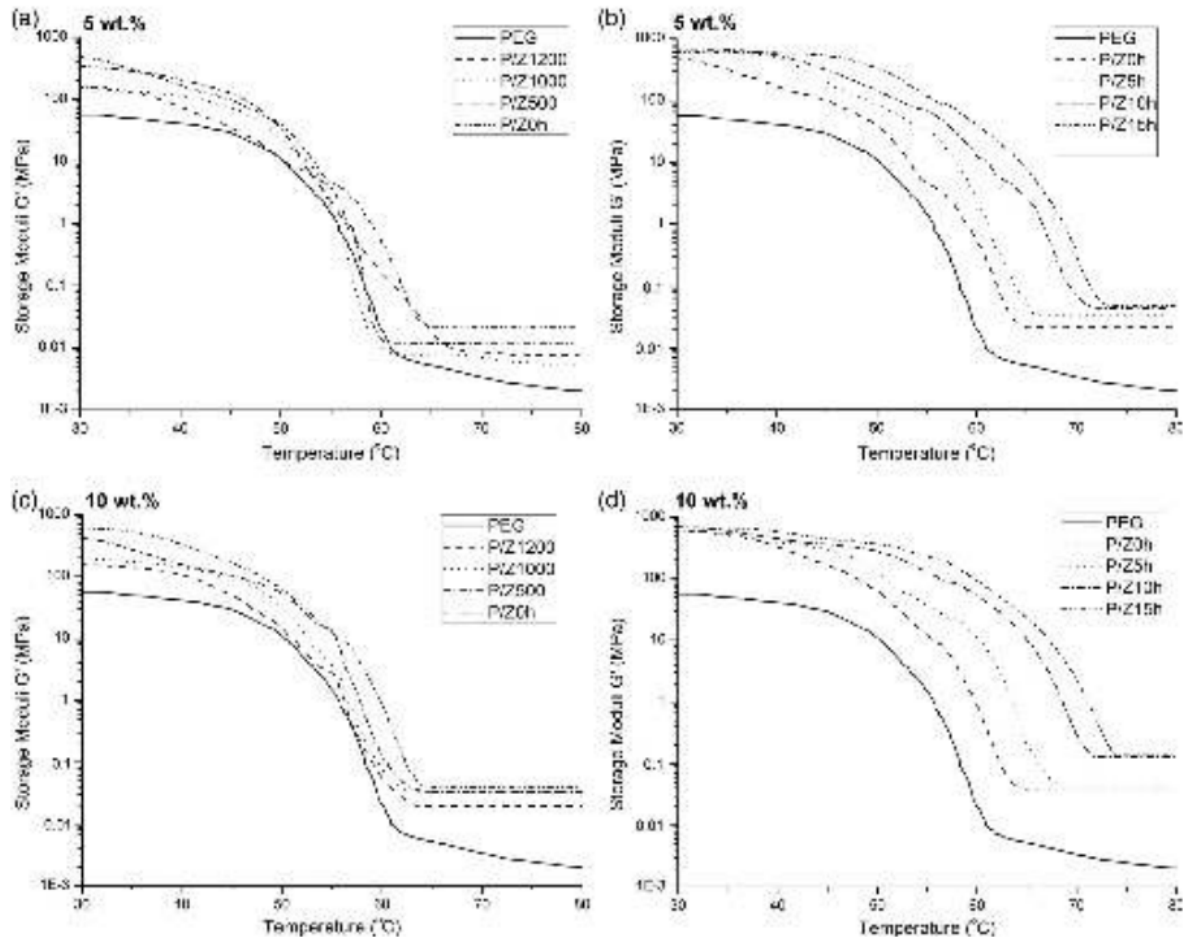


FIGURE 9 Storage moduli of PEG/zircon composites with varied zircon size and content of (a) microzircon 5 wt.%, (b) nanozircon 5 wt.%, (c) microzircon 10 wt.%, and (d) nanozircon 10 wt.%

effect of zircon size on the room-temperature (ambient)  $G'$  (see Table 4). In general, the smaller the size is, the larger the ambient  $G'$  value. For example, composites P/Z1200 and P/Z1000 with zircon sizes of 391 and 321 nm exhibit  $G'$  values 60–70% above that of pure PEG, while composites PZ10 and PZ15 with zircon sizes of 50 and 33 nm have  $G'$  values approximately 6–7 times that of pure PEG. As an example, when comparing  $G'$  values at 30°C, those of 5 wt.% P/Z1200 and P/Z5h composites increased from 154.90 MPa to 576.43 MPa. Furthermore, the plots for the submicron and nanosized composites (Z500, Z0, and Z5h) increase systematically over the entire region. These results imply that the thermomechanical properties of the composites are a result of surface contact-level behavior between the zircon filler and PEG as the matrix. Moreover, these results also illustrate differences in interfacial bonding between

the PEG polymer chains and zircon filler, which then reduce the freedom of movement of the chains. The smaller the zircon size is, the greater the interaction area between the chains and the filler. The consequence of the smaller filler size in exhibiting large surface contact and interaction with its surroundings is proven here. When the contact area between zircon and PEG is larger, the interfacial bonding between them increases. Nanozircon particles further restrict the motion of the polymer segments by reducing the slip of the main polymer chains. As a result, for smaller filler sizes, the free movement of polymeric molecules decreases, and hence, the storage modulus or the mechanical strength of the composites improves. The reinforcement mechanism in the composites is shown in Figure 8.

Another view of the effect of filler size can be explained by comparing the morphology of the

interaction area between the matrix and the filler. As the PEG thermoplastic polymer melts, the filler will act as a solidification initiator for the polymer. This process will create two areas around the filler, that is, the surrounding zone with a high modulus enriched layer and the depleting zone with a low modulus (Figure 10). The regions for small and large fillers are different. Small nanozircon particles will cover the surrounding (high modulus) zone, whose width is almost the same as the filler diameter, so that the reinforcement will be optimum. On the other hand, microzircon will have a narrower surrounding zone than the filler diameter and will cause a relatively lower increase in the storage modulus. Composites with medium-sized filler exhibit a combination of both effects.<sup>23</sup> This morphology interaction explanation is in line with the  $G'$  values, as shown in Figure 9.

Theoretically, the influence of filler size in increasing  $E'$  (hence  $G'$ ) of polymer-based composites was also reported by Amadji et al.,<sup>24</sup> who formulated the maximum stress of composites ( $\sigma_{c \max}$ ):

$$\sigma_{c \max} = \frac{4F_{c \max}}{\pi D^2} \quad (1)$$

TABLE 4 Room temperature shear storage moduli of PEG/zircon composites with varied zircon size and content

Samples	$G'$ (MPa)	
	5 wt. %	10 wt. %
PEG	93	93
P/Z1200	155	156
P/Z1000	159	217
P/Z500	338	459
P/Z0h	546	643
P/Z5h	576	636
P/Z10h	679	706
P/Z15h	593	684

where  $F_{c \max}$  is the external force, and  $D$  is the diameter of the filler. Thus, since  $G'$  is proportional to  $E'$ ,  $G' \propto \frac{1}{D^2}$ .

From here, in general, the smaller the filler size ( $D$ ), the higher the storage moduli. In addition, Chuayjuljit et al.<sup>25</sup> found that the storage modulus ( $E'$ ) was influenced by the particle size and the amount of filler. When small-sized carbon black (N550 with a particle size of 40–48 nm) and calcium carbonate (with a particle size of 390 nm) were added (60 part per hundred rubber, phr),  $E'$  increased 300% and 100%, respectively, compared with unfilled natural rubber. Therefore, the shear storage moduli ( $G'$ ) of PEG/zircon increase with reduced zircon size.

The filler composition also has a great effect on the strength of the composite. As shown in Table 4 and Figure 9, composites with the same size will have a higher  $G'$  at 10 wt.% zircon content. The presence of zircon increases the number of secondary bonds between PEG and zircon through van der Waals interactions. These secondary bonds prevent the free movement of the polymer when the composites are subjected to temperature and external forces. This phenomenon applies to all composites, with both micro and nanofillers.

In general,  $G'$  decreases with temperature because the energy stored due to molecular movements of the polymer chains increases.<sup>26</sup> When the temperature reaches the critical melting temperature,  $T_m$ , the carbon bond in the polymer group will weaken. As shown in Figure 9, a significant decrease in PEG occurs at temperatures of approximately 40–60°C. The addition of zircon filler to the composite can increase  $T_m$  up to approximately 65–70°C. We confirm that these  $T_m$  values are similar to those of DSC.<sup>16,27</sup> In addition, Figure 11 shows the  $\tan \delta$  plots from DMA, and the data are tabulated in Table 4.

Filler dispersibility also impacts the storage moduli. There are unexpected declines in the  $G'$  values of sample P/Z15h compared with sample P/Z10h, that is, as much

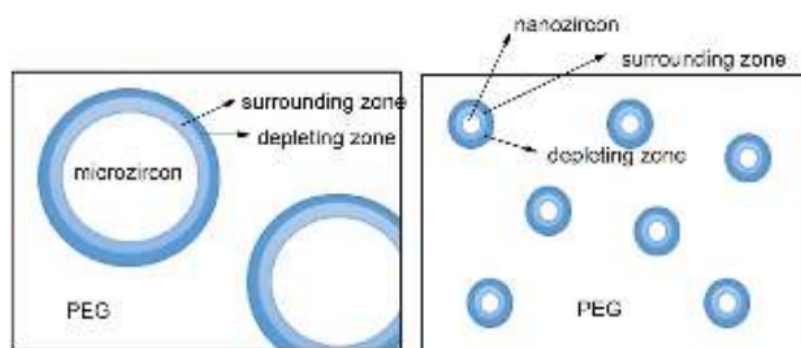
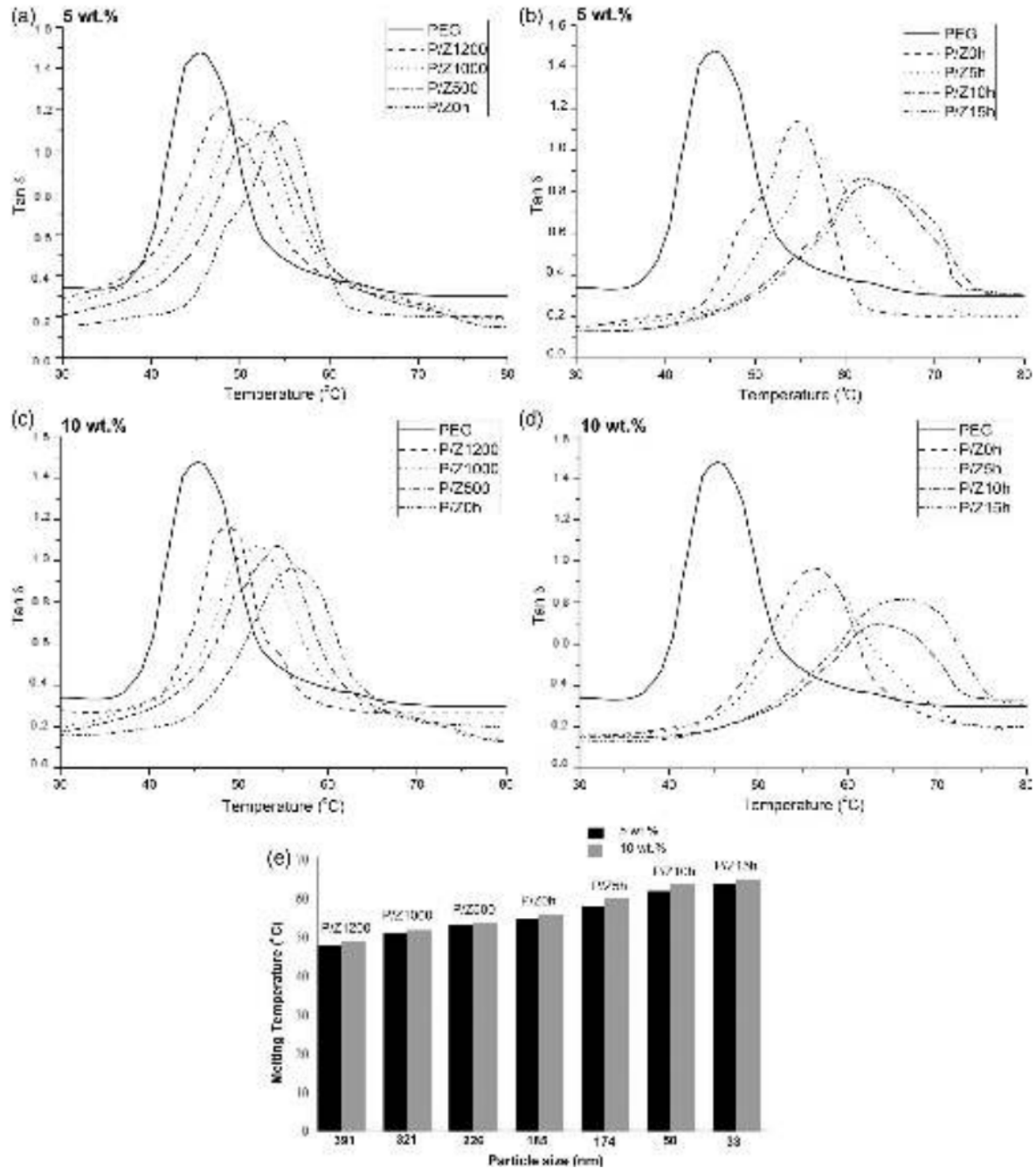


FIGURE 10 The morphological illustration of interaction zones of micro and nanozircon with PEG [Color figure can be viewed at [wileyonlinelibrary.com](http://wileyonlinelibrary.com)]



**FIGURE 11**  $Tan \delta$  plots of PEG/zircon composites (in varied zircon size) from (a) microzircon 5 wt.%, (b) nanozircon 5 wt.%, (c) microzircon 10 wt.%, (d) nanozircon 10 wt.%, and (e) the relation of  $T_m$  and particle size of zircon

as 25 and 22 MPa for 5 and 10 wt.% filler, respectively. Filler agglomeration in some parts of the composite may be the reason for this decrease, which is evident from SEM observations (Figure 6(c)) and zircon dispersibility

analysis (Table 3). Sample P/Z10h has the highest homogeneity, as shown by the lowest dispersibility index. Thus, zircon dispersibility influences the storage modulus of the composites.

### 3.5 | *Tan δ* and melting temperature ( $T_m$ )

The next thermomechanical feature is  $\tan \delta$  (see the plots in Figure 11), which describes the ratio between the loss ( $G''$ ) and storage moduli ( $G'$ ). In this study,  $\tan \delta$  is used to describe in detail the thermomechanical properties of PEG/zircon composites as well as the melting point of the matrix. The plots are compared in terms of their position, height, width, and shape.

#### 3.5.1 | Position

The highest peak of a  $\tan \delta$  plot can be associated with a transition temperature – in our case, the melting temperature  $T_m$  of PEG. The  $\tan \delta$  plots are given in Figure 11 (a)–(d), and the extracted  $T_m$  values for various filler sizes are shown in Figure 11(e). In general, three facts can be drawn here: (a) the presence of a filler increases the  $T_m$  value of PEG, (b) more filler raises the  $T_m$ , and (c) a smaller filler causes a higher  $T_m$ .

The explanation can be described as follows. The higher latent heat of zircon than pure PEG (i.e., 237 J/g<sup>28</sup> and 0.297 J/g,<sup>29</sup> respectively) is responsible for the higher  $T_m$  of the composites. Latent heat here defines an enthalpic anomaly correlated with phase changes from solid to liquid. In the presence of zircon, when the composite is heated, some of the heat energy is absorbed by zircon, and hence, a higher temperature is required to cause PEG to melt. In a polymeric material with a higher  $T_m$ , there is less free movement of polymer chains due to the damping of the filler when temperature or external force is applied.

Further examination shows that  $T_m$  increases with smaller zircon filler (Figure 11(e)). In addition, by looking at the change in the  $\tan \delta$  peaks in Figure 11(a)–(d), there is a clear role of nanozircon in shifting the  $T_m$  to a higher value. The mechanism of  $T_m$  reduction can be addressed by the decrease of  $\pi$  bonds in PEG chains in the microzircon composites and their replacement with new interfacial bonding between nanozircon and PEG. Moreover, the hydrogen bonds of PEG, which has a flexible drift,<sup>16</sup> are reduced by the presence of microzircon and further by nanozircon, ultimately giving stronger PEG composites. A similar trend in the role of a small particle size was revealed by Zhao et al.,<sup>30</sup> who reported that at 20 wt.%, the EG3 (expanded graphite with a particle size of <1  $\mu\text{m}$ )-paraffin composite had a higher melting temperature than EG1 (expanded graphite with a particle size of 400  $\mu\text{m}$ ) and EG2 (expanded graphite with a particle size of 120  $\mu\text{m}$ ), that is, 26.34°C, 24.77°C, and 24.62°C, respectively, as shown by DSC data.

In order to explain the dependence of  $T_m$  on particle size, we can use the following equation<sup>1</sup>:

$$T_\alpha = K_f \ln S \quad (2)$$

where  $\alpha$  indicates a transition,  $K_f$  is a constant and  $S$  is the specific surface area of filler per gram. From Equation (2), the interface area plays an important role in determining the transition temperature. In the case of zircon-filled PEG with filler size variation, a smaller filler size exhibits a larger interface area and hence gives a substantial effect on  $T_m$ . From the bond formation point of view, the addition of a smaller zircon increases the crosslink density and shortens the van der Waals bonds, and hence increases  $T_m$ .

In addition, it is interesting to note that the presence of agglomeration is quite influential in lowering  $T_m$ , as seen in sample P/Z15h. Agglomeration may act as a cluster of microparticles and lead to the appearance of voids without PEG-zircon bonds. The  $T_m$  value of sample P/Z15h is only 2°C above that of sample P/Z10h and is close to those of the microzircon-filled PEG composites P/Z500 and P/Z0h (see Figure 11(c)). The influence of agglomeration on  $T_m$  for different materials has been widely studied by others. Seemen et al.,<sup>31</sup> for example, showed that agglomeration in SiO<sub>2</sub>-Al<sub>2</sub>O<sub>3</sub>-K<sub>2</sub>O systems led to a relatively significantly lower melting temperature than when agglomeration was absent.

#### 3.5.2 | Height

The microfillers exhibit a higher  $\tan \delta$  peak height than the nanofillers (Figure 11(a) and (c) versus Figure 11 (b) and (d)). This result is in accordance with that reported previously.<sup>32</sup> The difference can presumably be related to the higher amount of damping factor in the microfiller composites due to the energy dissipation from the free movement of the polymer chains when external forces and temperature were applied. A clearer explanation can be seen from Figures 11 and 12, where the height of the  $\tan \delta$  peak is in line with the peaks of the loss modulus plots. In a microscopic view, the increase in the hydrogen bond network<sup>33</sup> in the composites will introduce more crosslink density in the composites and eventually decrease the  $\tan \delta$  peak height. By the same token, the lower the filler content is, the lower the intensity of the  $\tan \delta$  peak height.

#### 3.5.3 | Width

Another obvious difference from the  $\tan \delta$  plots between micro and nanofillers is the width of the peaks. Further scrutinizing this aspect, the width of the peaks appears to

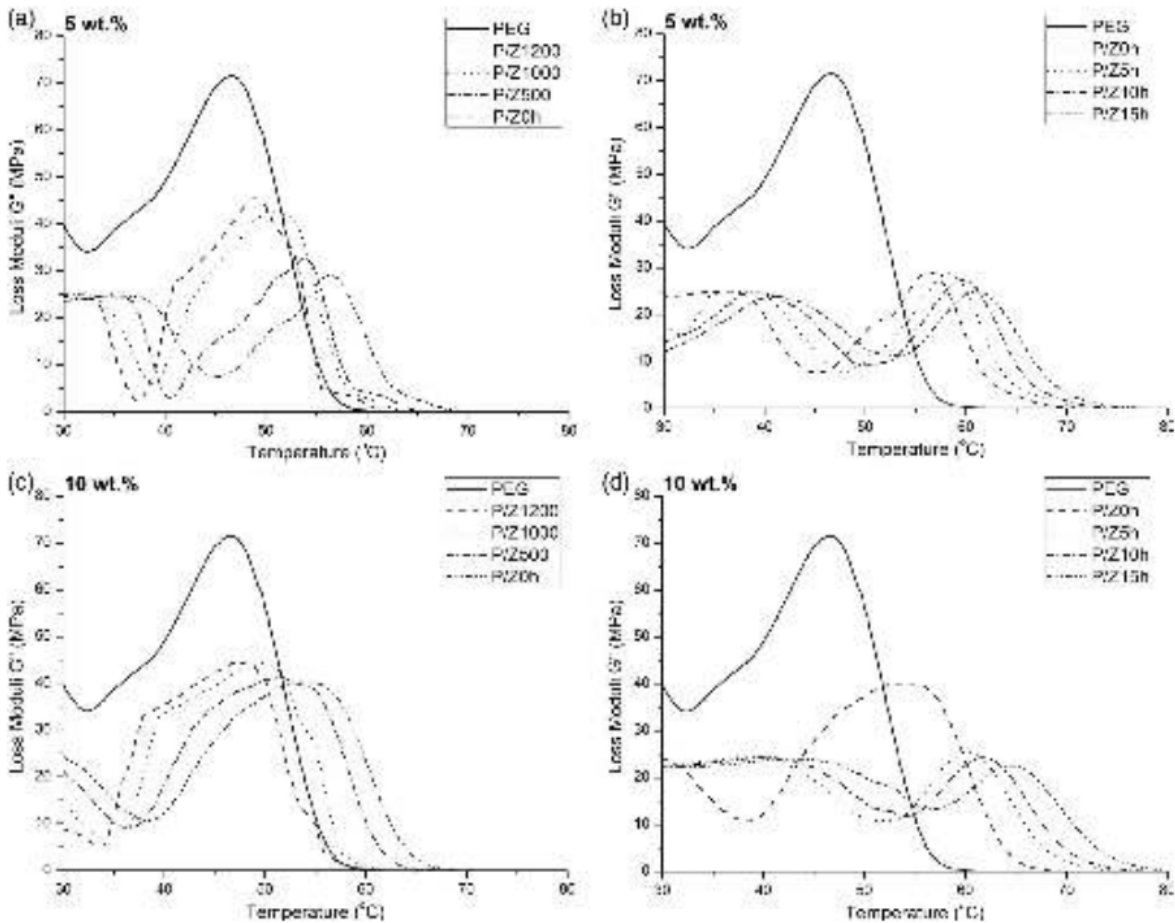


FIGURE 12 Loss moduli of PEG/zircon composites (in varied zircon size) from (a) microzircon 5 wt.%, (b) nanozircon 5 wt.%, (c) microzircon 10 wt.%, (d) nanozircon 10 wt.%

be greatly influenced by the size, distribution, and content of the filler and can be associated with the polymer crosslink density. The presence of filler induces a relatively slower softening of the polymer chain bonds because some of the applied energy is absorbed by the filler. In addition, the presence of a filler will increase the crosslink density of the composite, which results in an increase in stiffness and a decrease in dynamic losses due to the inhibited chain mobility. The higher the crosslink density is, the longer the relaxation time of the polymer chains. In general, these effects become more significant with increasing filler composition. In terms of peak width, the higher the filler content is, the wider the  $\tan \delta$  peak.<sup>34</sup>

$T_m$  also depends on the distribution of the filler. For more homogenous filler composites, as indicated by the  $I_{dispersability}$  values, the damping factor around  $T_m$  is dominated by the interaction between the filler and matrix, while for the less homogeneous filler composites, the interaction between the filler and filler dominates. As a

result, the homogeneous filler composites show broader  $\tan \delta$  peaks. For example (see Table 3), the zircon distribution in the P/Z10h composite is more homogenous than that in the P/Z1000 composite, and the former shows a wider  $\tan \delta$  pattern than the latter. Moreover, it appears that a microfiller will trigger stress localization around the unfilled PEG and create sudden damping, which leads to a sharp and relatively thin  $\tan \delta$  peak. This fact can be observed by comparing, for example, P/Z1200 and P/Z5h plots (Figure 11) around  $T_m$  and is based on the analogy of a more sudden yield strength<sup>34</sup> when polymer chains melt (deformed) at a lower temperature compared to those with nanofillers.

### 3.5.4 | Shape

Another interesting aspect is a relatively flatter  $\tan \delta$  peak maximum, as observed in the nanozircon filler composites,

than in the microzircon filler composites. At around  $T_m$ , the loss and storage moduli of the nanozircon composites compensate for each other, recalling that  $\tan \delta$  is the ratio between the two, to allow a slow change in  $\tan \delta$ . We argue here that the cause of the flat peak maximum is due to the shorter interparticle distance between fillers in the nanozircon composites. The deformation due to temperature at around  $T_m$  tends to be retained in the composites. Another possibility is that the shape of the  $\tan \delta$  plot may vary depending on the size distribution of the filler<sup>35</sup> and filler arrangement.<sup>34</sup> While a bell-like shape of  $\tan \delta$  is always expected, multisize particles may exhibit multiple temperature transitions that may broaden the peak or flatten the peak maximum. This characteristic is influenced by the molecular networks between PEG and zircon in the composites. A more heterogeneous filler promotes random networks and filling of the voids between particles with PEG. As a result, the shape of the  $\tan \delta$  plot slightly deviates from the ideal bell-like shape.

### 3.6 | <sup>16</sup> Loss modulus

The loss modulus ( $G''$ ) expresses the ability of a material to dissipate energy.<sup>36</sup> Figure 12 generally reveals that zircon reduces the energy loss in the composites compared to pure PEG. Moreover, there is a significant difference in the loss between the nano and microfiller composites. Around room temperature (30–40°C), the fluctuation of the loss modulus value of the microzircon composites is more visible. We argue that, as illustrated in Figure 10, the microzircon composites exhibit a narrow “surrounding zone” (area with the highest modulus) and cause the molecular chains of PEG to more easily vibrate when external force and temperature are applied. A similar phenomenon was also reported by Gan et al.,<sup>37</sup> where some fluctuations in the DMA initial loss modulus region were associated with carbon chain free movement and the temperature transition of cellulose powder as the filler.

As the temperature rises near  $T_m$ , the molecular segmental mobility of the PEG polymer is activated. Here, the intermolecular vibrations between polymer chains increase to reach the maximum and result in the degradation of PEG. The highest energy lost is shown by the maximum of a  $G''$  plot, which occurs near the melting temperature of a composite. Examining the loss modulus data from Figure 12, the addition of zircon as a filler (5 wt.% and 10 wt.%) was able to reduce the loss energy of the composites by half that of pure PEG. This  $G''$  drop has a good effect on the composite because more energy is stored and the energy lost due to internal friction and free movement of the PEG will be smaller, resulting in stronger composites in response to the applied

temperature and external forces. Furthermore, the results are in line with those of storage moduli and  $\tan \delta$  plots, as discussed previously. In addition, PEG with the lowest storage modulus has the highest energy lost ( $G''$ ). In previous research,<sup>17</sup> we succeeded in characterizing PEG/silica composites as PCMs and found that the energy dissipation decreased with the addition of silica fillers.

Figure 12 also shows that the loss modulus plots of the PEG/zircon composites are broadened, which can be associated with relaxation inhibition of the PEG polymer. When zircon is added, the PEG-zircon bonds will reduce the weak (flexible) O—H···O and C—H···O hydrogen bonds in the polymer. Relaxation of PEG is inhibited by the presence of zircon. Again, there is a slight difference between micro and nanozircon fillers. At the same zircon weight fraction, the nanozircon composites exhibit a larger volume fraction than the microzircon composites, so there will be more interfacial PEG-zircon bonds that inhibit the relaxation of PEG. As a result, the loss modulus peak of the nanozircon composites is wider.

In general, when comparing the thermomechanical data from PEG/zircon composites with various filler sizes, it is useful to note that the effectiveness of the zircon content in the PEG/zircon composites depends on the filler distribution. This agglomeration problem in nanopowder-filled composites requires further investigation.

## 4 | CONCLUSIONS


In this article, zircon powders with various sizes as fillers were successfully fabricated using heating and wet milling methods. Furthermore, PEG/zircon composites (with various zircon filler sizes) were also successfully synthesized with a relatively homogeneous filler distribution, except for the 5 and 10 wt.% P/Z15h composites, which showed agglomeration tendencies due to the relatively small filler size. In general, the smaller the size of the zircon, the greater the storage modulus of composites. The optimum value of storage modulus  $G'$  was obtained in the nanozircon composites, that is, with zircon milled for 10 h (Z10 h), giving values of 679.27 MPa and 706.37 MPa for 5 and 10 wt.%, respectively, or approximately 6–7 times of that of pure PEG. Meanwhile, the  $T_m$  values for the nanozircon-filled composite can reach nearly 20°C above that of pure PEG. With such a significant increase in storage modulus and  $T_m$ , PEG/zircon composites with nanofiller can be applied as energy storage materials.


### <sup>6</sup> ACKNOWLEDGMENTS

The authors would like to acknowledge the Ministry of Research and Technology/BRIN of the Republic of

Indonesia who provided to the research funding through World Class Research (No. 1055/PKS/ITS/2021).

## ORCID

Nur Aini Fauziyah  <https://orcid.org/0000-0002-9603-9828>

Suminar Pratapa  <https://orcid.org/0000-0003-2337-3566>

## REFERENCES

- [1] K. Iisaka, K. Shibayama, *J. Appl. Polym. Sci.* **1978**, *22*, 1321.
- [2] M. Miyazaki, T. Maeda, K. Hirashima, N. Kurokawa, K. Nagahama, A. Hotta, *Polymer* **2017**, *115*, 246.
- [3] S. Li, H. Wang, C. Chen, X. Li, Q. Deng, M. Gong, D. Li, *J. Appl. Polym. Sci.* **2017**, *134*, 45530.
- [4] P. B. Leng, H. Md Akil, O. Hui Lin, *J. Reinf. Plast. Compos.* **2007**, *26*, 761.
- [5] N. A. Fauziyah, T. A. Fadly, A. R. Hilmi, M. Mashuri, S. Pratapa, *IOP Conf. Ser. Mater. Sci. Eng.* **2019**, *496*, 012012.
- [6] Y. N. Baghdadi, L. Youssef, K. Bouhadir, M. Harb, S. Mustapha, D. Patra, A. R. Tehrani-Bagha, *J. Appl. Polym. Sci.* **2021**, *138*, 50533.
- [7] D. Zhao, H. Hamada, Y. Yang, *Composites, Part B* **2019**, *30*, 535.
- [8] E. Lizundia, V. A. Makwana, A. Larrañaga, J. L. Vilas, M. P. Shaver, *Polym. Chem.* **2017**, *8*, 3530.
- [9] Musyarofah, N. D. Lestari, R. Nurlaila, N. F. Muwwaqor, Triwikantoro, S. Pratapa, *Ceram. Int.* **2019**, *45*, 6639.
- [10] E. C. Subbarao, D. K. Agrawal, H. A. McKinstry, C. W. Salles, *J. Am. Ceram. Soc.* **1990**, *73*, 1246.
- [11] N. M. Rendtorff, S. Grasso, C. Hu, G. Suarez, E. F. Aglietti, Y. Sakka, *J. Eur. Ceram. Soc.* **2012**, *32*, 787.
- [12] N. F. Muwwaqor, N. A. Fauziyah, Musyarofah, Pratapa, *IOP Conf. Ser.: Mater. Sci. Eng.* **2018**, *432*, 012018.
- [13] S. R. Chauruka, A. Hassanpour, R. Brydson, K. J. Roberts, M. Ghadiri, H. Stitt, *Chem. Eng. Sci.* **2015**, *134*, 774.
- [14] L. Dawei, W. Feng, Z. Jianfeng, L. Dong, *Rare Metal Mater Eng* **2011**, *40*, 202.
- [15] L. D. Wulansari, N. A. Fauziyah, M. D. Nurmalasari, W. D. Handoko, M. Jawaidd, S. Pratapa, *Mater Today Proc* **2020**, *44*, 3285.
- [16] N. A. Fauziyah, A. R. Hilmi, T. A. Fadly, M. Z. Asrori, M. Mashuri, S. Pratapa, *J. Appl. Polym. Sci.* **2019**, *136*, 47372.
- [17] N. A. Fauziyah, A. R. Hilmi, M. Zainuri, M. Z. Asrori, M. Mashuri, M. Jawaidd, S. Pratapa, *J. Appl. Polym. Sci.* **2019**, *136*, 48130.
- [18] B. R. Rehani, P. B. Joshi, K. N. Lad, A. Pratap, *IJPAP Vol. February* **2006**, *44*, 2006.
- [19] U. Holzwarth, N. Gibson, *Nat. Nanotechnol.* **2011**, *6*, 534.
- [20] S. Gk, K. Ak, *Appl. Surf. Sci.* **2015**, *334*, 216.
- [21] Y. Li, F. Fang, Y. Song, Y. Li, D. Sun, S. Zheng, L. A. Bendersky, Q. Zhang, L. Ouyang, M. Zhu, *Dalton Trans.* **2013**, *42*, 1810.
- [22] S. Pratapa, T. Wahyuni, N. A. Fauziyah, G. A. Apriliyana, M. Mashuri, S. Firdaus, *J. Mech. Sci. Technol.* **2017**, *31*, 3653.
- [23] P. H. T. Vollenberg, D. Heikens, *Polymer* **1989**, *30*, 1656.
- [24] T. A. Amadji, E. C. Adjovi, J. Gérard, J. Barés, V. Huon, *HAL Archives Ouvertes* **2020**, *2*, 1. <https://hal.archives-ouvertes.fr/hal-02922025v2>.
- [25] S. Chuayjuljit, A. Imvittaya, N. Na-ranong, P. Patiyaraj, *Metals Mater. Miner* **2002**, *12*, 51.
- [26] A. J. Kinloch, R. D. Mohammed, A. C. Taylor, C. Eger, S. renger, D. Egan, *J. Mater. Sci.* **2005**, *40*, 5083.
- [27] C. A. Gracia-Fernandez, S. Gomez-Barreiro, J. Lopez-Beceiro, J. Saavedra, S. Naya, R. Artiaga, *Polym. Test* **2010**, *29*, 1002.
- [28] C. G. Robertson, C. J. Lin, M. Rackaitis, C. M. Roland, *Macromolecules* **2008**, *41*, 2727.
- [29] B. Tang, H. Wei, D. Zhao, S. Zhang, *Sol. Energy Mater. Sol. Cells* **2017**, *161*, 183.
- [30] Y. Zhao, L. Jin, B. Zou, G. Qiao, T. Zhang, L. Cong, F. Jiang, C. Li, Y. Huang, Y. Ding, *Appl. Therm. Eng.* **2020**, *171*, 115015.
- [31] A. Seemen; D. Atong; V. Sricharoenchaikul 2018 2nd International Conference on Green Energy and Applications (CGEA); **2018**; pp 268.
- [32] K. P. Menard, *Dynamic Mechanical Analysis*, 3rd ed., Taylor & Francis Group, Boca Raton **2008**.
- [33] J.-M. Huang, S.-J. Yang, *Polymer* **2005**, *46*, 8068.
- [34] H. Montes, F. Lequeux, J. Berriot, *Macromolecules* **2003**, *36*, 8107.
- [35] C. R. Szczepanski, C. S. Pfeifer, J. W. Stansbury, *Polymer (Guildf)* **2012**, *53*, 4694.
- [36] K. P. Menard, N. R. Menard, *Encyclopedia of Polymer Science and Technology*, John Wiley & Sons, Inc, Hoboken **2002**.
- [37] L. Gan, H. Guo, Z. Xiao, Z. Jia, H. Yang, D. Sheng, H. Pan, W. Xu, Y. Wang, *Polymers (Basel)* **2019**, *11*, 1982.

**How to cite this article:** N. A. Fauziyah, M. D. Nurmalasari, A. R. Hilmi, T. Triwikantoro, M. A. Baqiya, M. Zainuri, S. Pratapa, *J. Appl. Polym. Sci.* **2021**, e51565. <https://doi.org/10.1002/app.51565>



## 07. Filler-size-dependent dynamic mechanical properties of polyethylene glycol/zircon composites

---

### ORIGINALITY REPORT

---

6%

SIMILARITY INDEX

%

INTERNET SOURCES

%

PUBLICATIONS

6%

STUDENT PAPERS

---

### PRIMARY SOURCES

---

1	Submitted to Higher Education Commission Pakistan Student Paper	1%
2	Submitted to Korea University Student Paper	1%
3	Submitted to University of California, Merced Student Paper	1%
4	Submitted to University of Sheffield Student Paper	<1%
5	Submitted to Universitas Islam Indonesia Student Paper	<1%
6	Submitted to Surabaya University Student Paper	<1%
7	Submitted to Amrita Vishwa Vidyapeetham Student Paper	<1%
8	Submitted to Indian Institute of Technology, Kharagpure Student Paper	<1%

---

9	Submitted to University of Bath Student Paper	<1 %
10	Submitted to Heriot-Watt University Student Paper	<1 %
11	Submitted to National Institute of Technology Warangal Student Paper	<1 %
12	Submitted to Universitas Indonesia Student Paper	<1 %
13	Submitted to University College London Student Paper	<1 %
14	Submitted to Universiti Teknologi Petronas Student Paper	<1 %
15	Submitted to Hoa Sen University Student Paper	<1 %
16	Submitted to University of Bristol Student Paper	<1 %
17	Submitted to Kumoh National Institute of Technology Graduate School Student Paper	<1 %

Exclude quotes Off  
Exclude bibliography Off

Exclude matches Off